IEEE Photonics Journal
An IEEE Photonics Society Publication

Open Access

Phase Matching for Difference Frequency Generation in GaAs Via an Artificial Birefringence Technique Using Silver Nanowires

Volume 10, Number 3, June 2018

Naser Abdulhavid Otman
Michael Cada

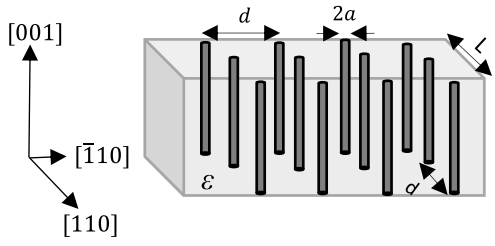

(a)

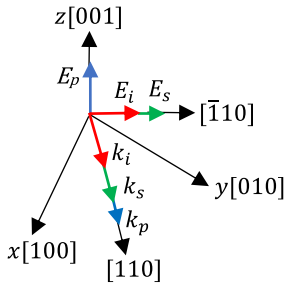

(b)

DOI: 10.1109/JPHOT.2018.2841983
1943-0655 © 2018 IEEE

Phase Matching for Difference Frequency Generation in GaAs Via an Artificial Birefringence Technique Using Silver Nanowires

Naser Abdulhavid Otman [1] **and Michael Cada** [1, 2]

[1]Department of Electrical and Computer Engineering, Dalhousie University, Halifax, NS B3H 4R2, Canada
[2]IT4Innovations, VSB-Technical University of Ostrava 708 33, Ostrava-Poruba, Czech Republic

DOI:10.1109/JPHOT.2018.2841983

Manuscript received March 7, 2018; revised May 22, 2018; accepted May 24, 2018. Date of publication May 30, 2018; date of current version June 13, 2018. This work was supported in part by the Natural Sciences and Engineering Research Council (NSERC) of Canada and in part by the European Regional Development Fund in the IT4Innovations National Supercomputing Center - Path to Exascale Project (Project CZ.02.1.01/0.0/0.0/16_013/0001791 within the Operational Programme Research, Development and Education. Corresponding author: Naser Abdulhavid Otman (e-mail: naser.otman@dal.ca).

Abstract: The lack of anisotropic properties in GaAs prevents the use of birefringence as a phase matching technique in three-wave mixing with GaAs as a nonlinear medium. When metallic nanowires are embedded in GaAs, the composite structure is characterized as a metamaterial with anisotropic properties, if the separation distance between the nanowires is less than the wavelengths of the mixed waves. The effective permittivity is used to investigate this metamaterial structure with its anisotropic properties theoretically in terms of phase matching for difference frequency generation. The resultant difference frequencies, which are in the mid-infrared region, are broadly tunable from 2.8 to 11 μm. This tuning is performed by varying the pump and the signal wavelengths in the range between 1 to 2 μm. The losses of the structure due to absorption are included using the transfer matrix method.

Index Terms: Nonlinear wave mixing, metamaterial, phase matching, semiconductors, metals.

1. Introduction

Phase matching, which involves momentum conservation of the photons, is the most important aspect to consider in nonlinear optical frequency mixing [1]. In general, phase matching requires the medium to be a non-dispersive material. Although the materials are dispersive, phase matching is achieved by using birefringence and quasi-phase matching techniques in media made of materials such as periodically poled lithium niobate (PPLN), potassium titanate phosphate (KTP), and barium borate (BBO). Difference frequency generation is used to generate optical frequencies that cannot be generated by using ordinary laser sources. Most difference frequency generation (DFG) based on parametric wavelength conversion uses nonlinear crystals, such as PPLN, KTP, BBO, and lithium niobate [2], [3]. GaAs and InP, with a cubic lattice structure from the III–V semiconductor group, are alternative for optical frequency mixing [4]. Optical mixing based on InP material for second

harmonic generation and optical rectification were experimentally verified for 1.55 μm fundamental wavelength [5]. GaAs, with larger second-order susceptibility $\chi^{(2)}$ and wide transparent infrared optical window, from 1 μm to 17 μm, is a better candidate for difference frequency generation [6]. Despite these advantages, it is not possible to use birefringence phase matching techniques with GaAs or InP, due to their isotropic properties.

There are other methods for achieving phase matching in III–V semiconductors with a cubic lattice structure, for difference frequency generation, such as quasi-phase matching, modal phase matching, domain-disordered quasi-phase matching, and suspended GaAs waveguides [6]–[10]. Tunable emissions from 6.7 μm to 12.7 μm have been demonstrated in a nonguided orientation patterned GaAs [11], and the longest wavelength was generated through DFG in AlGaAs waveguide from 7.5 μm to 8.5 μm [12].

Phase matching by using artificial anisotropy is possible if a strongly anisotropic structure can be obtained. Artificial birefringence using multi-layered GaAs/AlAs was first proposed by J. P. van der Ziel [13]. Relatively large birefringence has been demonstrated with the multilayer structure of oxidized GaAs/AlAs [14]. Phase matching has been achieved for parametric amplification of down conversion by using artificial birefringence in multilayer waveguides of oxidized GaAs/AlAs [15]. Phase matching has been demonstrated for a DFG by using artificial birefringence with a multilayer structure of GaAs/Al_x Ga_{1-x} As, with three layers of Al_x Ga_{1-x} As and one layer of GaAs [16]. Obtaining a large birefringence or a strongly anisotropic structure has been challenging. The use of an optical metamaterial with metallic nanowires is an alternative method of obtaining a strongly anisotropic structure [17]–[21]

In the present research, we performed a theoretical investigation of the phase matching aspect of DFG in a slab medium of a metamaterial structure of GaAs with permittivity ε_{GaAs} as the host material, with inclusions of periodic arrays of silver nanowires. To our knowledge, there have been no published attempts made to use nanowires with GaAs metamaterials structure for phase matching to generate mid-infrared wavelengths (terahertz frequencies).

2. Theory

The metamaterial structure that is composite of a dielectric and very thin periodic metallic wires could have an effective plasma frequency below the bulk plasma frequency which is generally in the ultraviolet (UV) range. The effective plasma frequency is changeable and could be reduced to IR, THz, or GHz by changing the period of the wires [22]–[24]. In metamaterial structures, where metal and dielectric nanoparticles are intermixed together within the scale of nanometers, finding the optical response of such structures by solving Maxwell's equations is impossible because of the complexity of the boundary conditions. An inhomogeneous structure with a scale less than the wavelength is treated as one macroscopically uniform medium using the approximation of the effective medium approach [17]. Under this approximation, the scattering response by individual metal and dielectric nanoparticles is determined from the average response of the whole system using the effective permittivity [17].

The geometry analyzed in this work is a slab of a composite structure of periodic arrays of silver nanowires of a period d and a radius a embedded in GaAs with electric permittivity ε_{GaAs} as a host medium, as shown in Fig. 1(a). Fig. 1(b) shows the Miller indices of the GaAs lattice structure as defined in Cartesian coordinates, and illustrates the polarizations and propagation of the three waves to be mixed. The three waves are defined as the pump wave ω_p, with electric field E_p; the signal wave ω_s, with electric field E_s; and the idler wave $\omega_i(\omega_i = \omega_p - \omega_s)$, with electric field E_i, where $\omega_p > \omega_s > \omega_i$.

We consider the applied waves at normal incidence to the wires, with the electric field polarized parallel to the wires along [001] for the pump wave E_p, and orthogonally polarized along [$\bar{1}$10] for the signal wave E_s. Based on the second order subspecialties $\chi^{(2)}_{xyz}$ and $\chi^{(2)}_{yzx}$ of GaAs, the resultant difference wave E_i will be orthogonally polarized along [$\bar{1}$10].

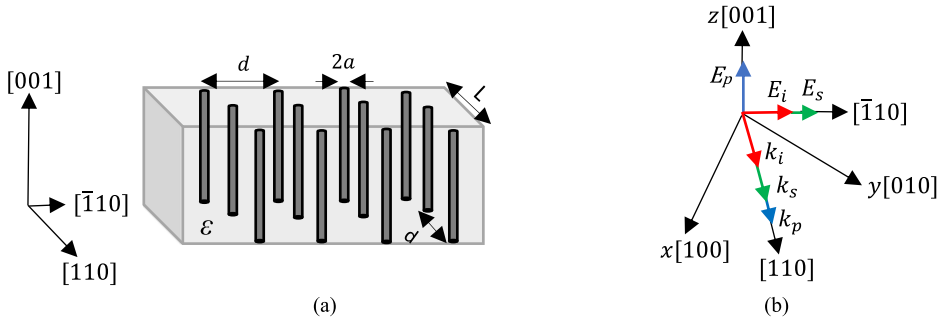

Fig. 1. (a) Structure of silver nanowires of period d embedded in GaAs medium of electric permittivity ε_{GaAs}, with a thickness $L = Nd$, and semi-infinite height and width, where N is the number of wires columns. (b) Illustration of Miller indices of GaAs lattice structure with Cartesian coordinates, wave propagation directions, and polarizations.

If the waves are propagating orthogonally to the wires and the electric field is parallel, with the limit $d \ll \lambda$, the effective permittivity of the structure in the direction parallel to the wires can be modeled by lossy Drude model [22]–[24] as,

$$\varepsilon_z = \varepsilon^{\parallel} = \varepsilon_{GaAs}\left[1 - \frac{\omega_{plasma}^2}{\omega\left(\omega + i\gamma_{\text{eff}}\right)}\right] \tag{1}$$

$$\gamma_{\text{eff}} = \frac{\varepsilon_0}{\sigma}\frac{2c^2}{a^2 \ln\left(d/a\right)}, \quad \omega_{plasma} = \frac{1}{\varepsilon_{GaAs}}\frac{2\pi c^2}{d^2 \ln\left(d/a\right)} \tag{2}$$

Here γ_{eff} is the effective damping frequency, ω_{plasma} is the effective plasma frequency, and σ is the static conductivity of silver. The effective damping frequency γ_{eff} strongly depends on the wires radius a, which offers more degree of freedom to modify the absorption properties of the structure. If the wires radii are very thin compared to the wavelength ($a \ll \lambda$), their orthogonal polarization can be neglected, and the orthogonal permittivity will be the same as the host medium ε_{GaAs} [25],

$$\varepsilon_x = \varepsilon_y = \varepsilon^{\perp} = \varepsilon_{GaAs} \tag{3}$$

The TE polarization has the electric field directed along the z-axis; and the TM polarization has the electric field oriented parallel to the xy plane, which thus has components in x the and y directions. The idler wave ω_i and the signal wave ω_s are TM polarized with wavevectors k_i and k_s, respectively. They propagate in the plane xy, making an angle of 45° with respect to the x and y axes. The pump wave ω_p is TE polarized in the z-direction with a wavevector k_p according to the following type-I coupling interaction:

$$E_p\left(TE\right) - E_s\left(TM\right) \overset{\chi^{(2)}_{xzy}=\chi^{(2)}_{yzx}}{\Rightarrow} E_i\left(TM\right) \tag{4}$$

Type-I coupling is a polarization configuration where the signal polarization is parallel to the idler polarization; while in type-II, the signal and the idler polarizations are orthogonal [26]. Efficient difference frequency generation requires large second-order susceptibility $\chi^{(2)}$ and phase matching between the three wavevectors; $k_p(\omega_p)$, $k_s(\omega_s)$, and $k_i(\omega_i)$. The phase matching condition is expressed in terms of the wavevectors as $\Delta k = k_p(\omega_p) - k_s(\omega_s) - k_i(\omega_i)$.

This structure can be successfully fabricated using electrochemically growing of metallic nanowires in porous alumina template [27]–[30], where the holes are filled with the metals such as silver (Ag). In the following stage the host alumina matrix is removed, and the free-standing wires are filled with another material such as GaAs [29], [30].

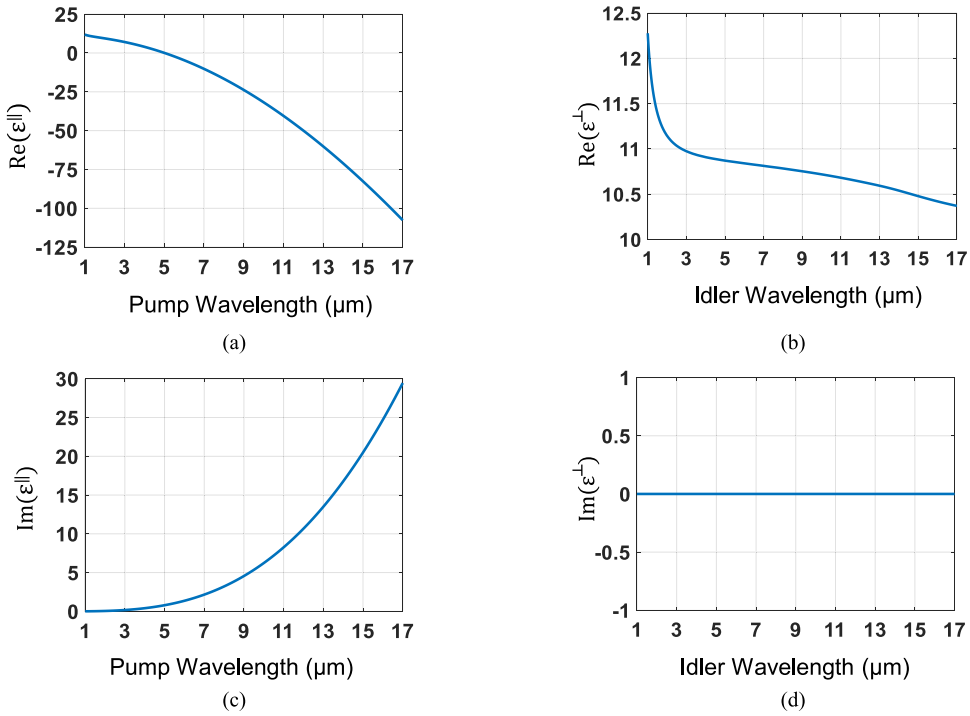

Fig. 2. Parallel and perpendicular permittivities $\varepsilon^{\parallel}$ and $\varepsilon^{\perp}$ for wires dimeter $2a = 35$ nm and period $d = 350$ nm; (a), (b) real parts of parallel and orthogonal permittivities. (c), (d) imaginary parts of parallel and orthogonal permittivities.

3. Results and Discussions

We investigated the structure within the optical transmission window of GaAs, in the spectral region from 1 μm to 17 μm. The pump wave has the shortest wavelength, the idler wave has the longest wavelength, and the wavelength of the signal wave is between the other two. The structure is tuned by varying the pump wave frequency ω_p and the signal wave frequency ω_s. The idler wave is the wave with the difference frequency $\omega_i = \omega_p - \omega_s$ that satisfies the phase matching condition. We used experimentally measured data for GaAs permittivity [31]. The structure parameters values have been chosen for the diameter $2a = 35$ nm and the period $d = 350$ nm, as a compromise between the absorption and the longest achievable difference frequency at the matching.

Fig. 2 shows the real and imaginary parts of the parallel and the orthogonal permittivities $\varepsilon^{\parallel}$ and $\varepsilon^{\perp}$. As the pump wave is parallel polarized, the real and imaginary parts of the parallel permittivity are plotted with respect to the pump-wave wavelengths; at the same time, the orthogonal permittivity is plotted with respect to the idler-wave wavelengths or the signal-wave wavelengths because of their orthogonal polarization. The orthogonal permittivity is just the plot of the experimental measured data of GaAs permittivity, with only the real part values and neglecting the imaginary part [31]. The silver conductivity in Eq. (2) is $6.28^{*}10^{7}\Omega^{-1}\mathrm{m}^{-1}$.

To examine the phase matching aspect, it is necessary to deal with the refractive indices, $n^{\parallel} = Re(\pm\sqrt{\varepsilon^{\parallel}})$ and $n^{\perp} = Re(\pm\sqrt{\varepsilon^{\perp}})$. The square root has two possible solution values, positive or negative (negative refractive index). Since the orthogonal permittivity is the permittivity of GaAs ($\varepsilon^{\perp} = \varepsilon_{GaAs}$), this indicates a positive refractive index. In the case of the parallel permittivity $\varepsilon^{\parallel}$, the causality requires the imaginary part of the refractive index to be positive for any passive material [17], [32], [33], which results in a positive refractive index. Fig. 3 shows the parallel and perpendicular refractive indices. The parallel refractive index $n^{\parallel}$ has strongly dispersive properties because of the effect of the metal nanowires, while the perpendicular $n^{\perp}$, which is the experimentally measured data of the refractive index of GaAs [31], is less dispersive. These contrasting refractive indices

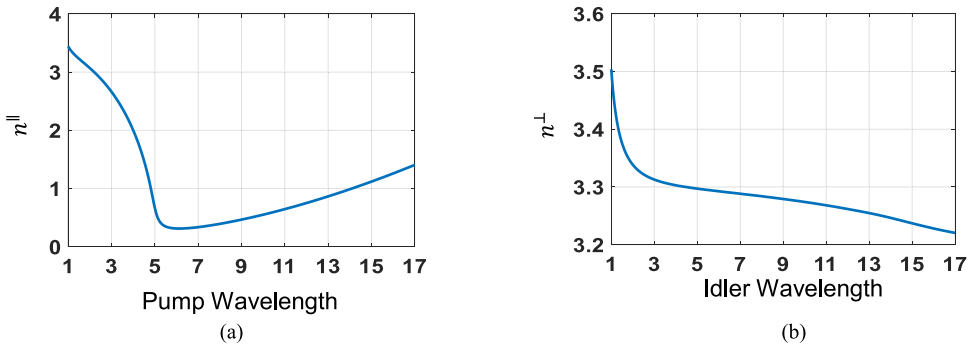

Fig. 3. Parallel $n^{\parallel}$ and orthogonal $n^{\perp}$ indices for wires dimeter $2a = 35$ nm and period $d = 350$ nm; (a) parallel index, (b) orthogonal index.

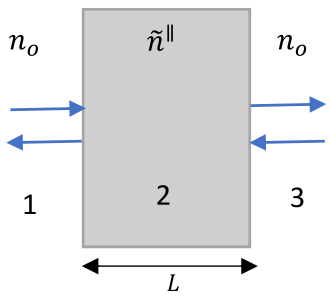

Fig. 4. Three layers system to find reflectance R and transmittance T.

along the principle axes provide a possibility of achieving phase matching for three waves mixing and, specifically, generating frequencies in the mid-infrared region.

The transfer matrix method was used to compute the absorption through the structure medium as it is treated as macroscopically uniform medium [17], with a complex effective refractive index $\tilde{n}^{\parallel} = \sqrt{\varepsilon^{\parallel}}$. The system is three layers media as shown in Fig. 4. The structure of thickness L and complex refractive index $\tilde{n}^{\parallel}$ is impressed in a layer of index n_o. Three transfer matrices needed to find and multiplied to get the complete transfer matrix.

First, we find the transfer matrices at the two interfaces:

$$M_{12} = \frac{1}{t_{12}} \begin{bmatrix} 1 & r_{12} \\ r_{12} & 1 \end{bmatrix} \tag{5}$$

$$M_{23} = \frac{1}{t_{23}} \begin{bmatrix} 1 & r_{23} \\ r_{23} & 1 \end{bmatrix} \tag{6}$$

The transfer matrix of the structure layer between the interfaces is as following:

$$M_2 = \begin{bmatrix} e^{j\delta} & 0 \\ 0 & e^{-j\delta} \end{bmatrix} \tag{7}$$

Where $r_{12} = -r_{23} = r = \frac{n_o - \tilde{n}^{\parallel}}{n_o + \tilde{n}^{\parallel}}$, $t_{12} = \frac{2n_o}{n_o + \tilde{n}^{\parallel}}$, $t_{23} = \frac{2\tilde{n}^{\parallel}}{n_o + \tilde{n}^{\parallel}}$, and $\delta = \frac{2\pi}{\lambda}\tilde{n}^{\parallel}L$. The complete transfer matrix $M = M_{12}M_{23}M_2$:

$$M = \begin{bmatrix} b_{11} & b_{12} \\ b_{21} & b_{22} \end{bmatrix} = \frac{e^{j\delta}}{t_{12}t_{23}} \begin{bmatrix} 1 - r^2 e^{-j2\delta} & -r(1 - e^{-j2\delta}) \\ r\left(1 - e^{-j2\delta}\right) & -r^2 + e^{-j2\delta} \end{bmatrix} \tag{8}$$

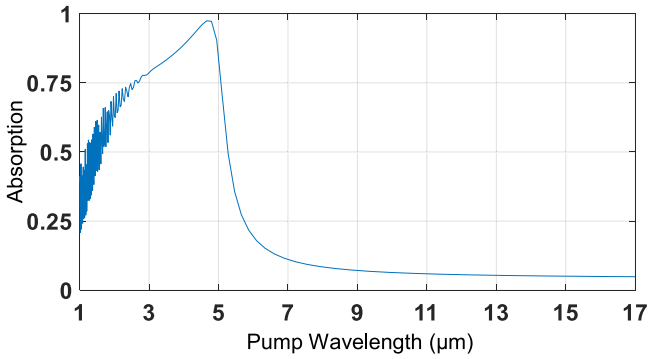

Fig. 5. Absorption of structure for wires diameter $2a = 35\ nm$, period $d = 350$ nm, $n_o = 1$, and thickness $L = Nd = 35\ \mu$m with $N = 100$ (number of wire columns).

This three -layers system behaves as Fabry-Perot etalon illuminated by one incident light from the left of the structure, then the reflectance R and transmittance T are defined from the matrix M as following:

$$R = \left|\frac{b_{21}}{b_{11}}\right|^2 = \left|\frac{r\left(1 - e^{-j2\delta}\right)}{1 - r^2 e^{-j2\delta}}\right|^2 \tag{9}$$

$$T = \left|\frac{1}{b_{11}}\right|^2 = \left|\frac{t_{12}t_{23}e^{-j\delta}}{1 - r^2 e^{-j2\delta}}\right|^2 \tag{10}$$

Fig. 5 shows the absorption $A = 1 - R - T$ of the structure for thickness $L = Nd = 35\ \mu$m with $N = 100$ (number of wire columns), where $d = 350$ nm. R is the reflectance, and T is the transmittance, assuming $n_o = 1$ for the surrounding medium. The pump waves whose electric field is parallel to the wires experience absorption, while the signal and idler waves whose electric fields are orthogonal to the wires do not experience absorption due to neglecting the orthogonal polarization of the thin wires [25].

It is obvious from the real part of the parallel permittivity $Re(\varepsilon^{\parallel})$ in Fig. 2(a), or the absorption A in Fig. 5, that the plasma wavelength of the structure, $\lambda_{plasma} = c/\omega_{plasma}$, is around 5 μm. The absorption is extremely high at the plasma wavelength, while in the region of the wavelengths that are much shorter than the plasma wavelength ($\lambda \ll \lambda_{plasma}$) the absorption is low, in which case the real part of the parallel permittivity is positive, the imaginary part is very small, and the optical transmission is dominant. In the region where the wavelengths are much longer than the plasma wavelength, the optical reflection is dominant. The pump-wave wavelengths λ_p that satisfy the phase matching are in the range of the spectrum from 1 μm to 1.2277 μm, which are shorter in wavelength than the plasma wavelength.

In the spectrum region $\lambda < 3\ \mu m$, narrow oscillations (Fabry–Perot oscillations) occur in the absorption. These oscillations exist because of the coherent interference between the partial internal reflected waves. The oscillations disappear in the spectrum region $\lambda > 3\ \mu m$ because the imaginary part of the parallel permittivity $Im(\varepsilon^{\parallel})$ in Fig. 2(c) becomes valuable, thus the absorption resonance starts to dominate, while the partial internal reflections will disappear.

Based on the refractive indices, we can determine the phase mismatch between the waves according to:

$$\Delta k = n^{\parallel}(\omega_p)\frac{\omega_p}{c} - n^{\perp}(\omega_s)\frac{\omega_s}{c} - n^{\perp}(\omega_i)\frac{\omega_i}{c} \tag{11}$$

The phase mismatch Eq. (11) was tested by varying the pump frequency ω_p and signal frequency ω_s. When the phase mismatch $\Delta k = 0$, the difference frequency ω_i is assigned to be the third frequency that satisfies the conservation of energy and momentum.

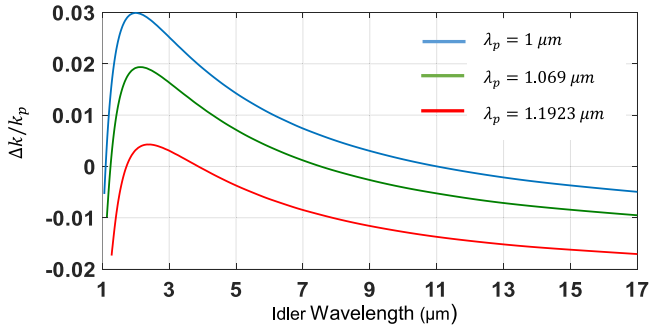

Fig. 6. Mismatch plot ($\Delta k/k_p$) as function of idler wavelength λ_i at three different values of pump wavelengths $\lambda_p = 1\ \mu$m, 1.069 μm, and 1.1923 μm, where $\Delta k = k_p - k_s - k_i$ and k_p is wavevector of the pump signal. Matching is achieved at the signal wavelengths $\lambda_s = 1.0997\ \mu$m, 1.2455 μm, and 1.7222 μm, respectively. Resulting idler wavelengths are $\lambda_i = 11.033\ \mu$m, 7.5406 μm, and 3.875 μm, respectively.

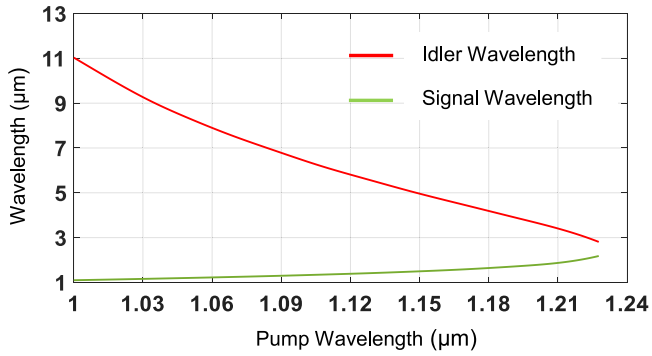

Fig. 7. Tuning relationship between three wavelengths that satisfy the phase matching condition. Pump wavelengths vary from 1 μm to 1.2277 μm, signal wavelengths change from 1.0997 μm to 2.1809 μm, and idler wavelength extend from 11.033 μm to 2.8091 μm.

Fig. 6 shows the case of the phase mismatch plot ($\Delta k/k_p$) as a function of the idler wavelength λ_i, at three different values of the pump wavelengths $\lambda_p = 1\ \mu$m, 1.069 μm, and 1.1923 μm. It was found that the phase matching is satisfied at the following idler wavelengths $\lambda_i = 11.033\ \mu$m, 7.5406 μm, and 3.875 μm, respectively. The corresponding signal wavelengths at the matching are $\lambda_s = 1.0997\ \mu$m, 1.2455 μm, and 1.7222 μm, respectively. The tuning relationship between the three wavelengths that satisfied the phase matching and the energy conservation in the entire spectrum from 1 μm to 17 μm is shown in Fig. 7.

It is clear from this tuning relationship that the possible tuned range of the idler wavelengths, which is in the mid-infrared range, is broad, and extends from 11 μm as the longest wavelength to the shortest wavelength of 2.8 μm. The pump-wave wavelengths vary from 1 μm to 1.2277 μm, while the signal-wave wavelengths changes from 1.0997 μm to 2.1809 μm. This is a very interesting result since the pump and the signal wavelengths lie in the spectrum region from 1 μm up to 2 μm, in which the conventional tunable laser sources are available.

Nonlinear conversion processes are generally very weak due to small nonlinear coefficients of materials. The conversion efficiency at phase matching $\Delta k = 0$ in a plane-wave approximation, nondepleted pump approximation, and including the effects of linear absorption is given by [34]:

$$\eta = \frac{P_i}{P_s} = \eta^o e^{\left[-(\alpha_p+\alpha_s+\alpha_i)L/2\right]} \frac{\sinh^2\left[(\alpha_p+\alpha_s-\alpha_i)L/4\right]}{\left[(\alpha_p+\alpha_s-\alpha_i)L/4\right]^2}, \quad \eta^o = \frac{8\pi^2 d_{\text{eff}}^{(2)} L^2 I_p}{\varepsilon_o n_p n_s n_i c \lambda_i^2} \tag{12}$$

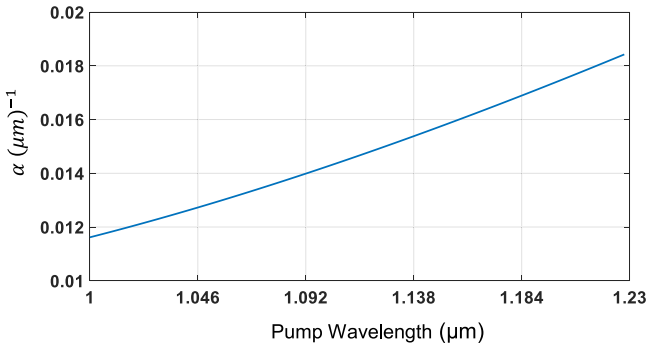

Fig. 8. Absorption coefficient α with respect to the pump wavelength for $L = 35\ \mu$m and $d = 350$ nm.

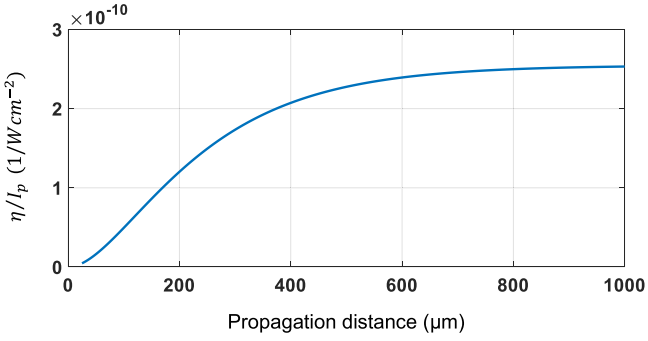

Fig. 9. Normalized efficiency η/I_p.

η^o is the lossless efficiency. α_p, α_s, and α_i are absorption coefficients for pump, signal, and idler waves, respectively. n_p, n_s, and n_i are refractive indices for pump, signal, idler waves, respectively. If the signal and the idler waves absorptions are neglected because of their negligible interaction to the tiny nanowires, the normalized efficiency to the pump intensity I_p is given as:

$$\frac{\eta}{I_p} = \frac{8\pi^2 d_{\text{eff}}^{(2)} L^2}{\varepsilon_o n_p n_s n_i c \lambda_i^2} e^{\left(\frac{-\alpha^{\parallel} L}{2}\right)} \frac{\sinh^2\left(\frac{\alpha^{\parallel} L}{4}\right)}{\left(\frac{\alpha^{\parallel} L}{4}\right)^2} \tag{13}$$

$\alpha^{\parallel}$ is the absorption coefficient along the nanowires, and $\alpha^{\parallel} = \alpha_p = 4\pi * im(\sqrt{\varepsilon^{\parallel}})/\lambda_p$. Fig. 8 shows the absorption coefficient $\alpha^{\parallel}$ versus the pump wavelength at phase matching, from 1 μm to 1.2277 μm. Absorption causes a propagation loss to the pump wave of 0.05 dB/μm at the wavelength of 1 μm, and 0.075 dB/μm at wavelength 1.2 μm.

Fig. 9 shows the normalized efficiency η/I_p versus the propagation length with the following parameters: $\lambda_i = 11\ \mu m$, $n_p = 3.4415$, $n_s = 3.4591$, $n_i = 3.2678$, and $d_{\text{eff}}^{(2)} = 370$ pm/V [1]. The efficiency is very week and limited with the propagation distances because of the ohmic loss at the pump wavelengths. Larger refractive indices and longer idler wavelengths decrease the efficiency. This efficiency could be higher if pump depletion is assumed. Practically, the propagation loss of metallic nanowires, e.g., silver, is much less than the theoretically calculated [35]. We expect, based on the results in [35], the propagation loss in our structure be much less than theoretically calculated; this will increase the efficiency as well as the propagation length.

4. Conclusion

We have investigated the phase matching condition for DFG by using a composite structure of metamaterial of mixing GaAs as a nonlinear material with periodic arrays of silver nanowires. The structure exhibits extreme optical anisotropy along the principle axes due to the higher parallel polarization along the wires compared with the orthogonal polarization. Phase matching was achieved for generating tunable broad mid-infrared wavelengths from 2.8 μm to 11 μm. The pump and the signal wavelengths lie in the spectrum range from 1 μm to 2 mum. The absorption by metallic nanoparticles is a challenging problem in metamaterials. Here, we applied the pump wave of the shortest wavelengths, from 1 μm to 1.2277 μm, as parallel polarized wave along the wires, in which the absorption is minimum. To shift the spectrum, the period ***d*** should be changed to larger values for the redshift and lower for the blueshift.

This investigated region of the mid-infrared from 2.8 μm to 11 μm is a part of the mid-infrared spectrum $3 - 20$ μm, which is very interesting in science and technology. It is the wavelengths region of vibrational resonances of many molecules, making the mid-infrared sources very important in spectroscopy, chemical and biomolecular sensing. Also, it lies in the two of the optical transmission windows of the atmosphere 3–5 μm and 8–13 μm, which are important in remote sensing.

References

[1] R. W. Boyd, *Nonlinear Optics*, 3rd ed. New York, NY, USA: Academic, 2008.
[2] S. J. Wagner *et al.*, "Difference frequency generation by quasi-phase matching in periodically Intermixed semiconductor superlattice waveguides," *IEEE J. Quantum Electron.*, vol. 47, no. 6, pp. 834–840, Jun. 2011.
[3] M. Cada, J. He, R. Normandin, H. Dai, and S. Janz, "Optical nonlinear devices," *Int. J. Nonlinear Opt. Phys.*, vol. 3, no. 2, pp. 169–203, 1994.
[4] M. Cada, "Nonlinear optical devices (Invited Paper)," *Optica Pura y Aplicada*, vol. 38, no. 3, pp. 1–10, 2005.
[5] M. Cada, "Optical harmonic mixers," *IEEE J. Quantum Electron.*, vol. 31, no. 2, pp. 269–277, Feb. 1995.
[6] A. S. Helmy *et al.*, "Recent advances in phase matching of second-order nonlinearities in monolithic semiconductor waveguides," *Laser Photon. Rev.*, vol. 5, no. 2, 2010, pp. 1–15.
[7] S. J. B. Yoo, C. Caneau, R. Bhat, M. A. Koza, A. Rajhel, and N. Antoniades, "Wavelength conversion by difference frequency generation in AlGaAs waveguides with periodic domain inversion achieved by wafer bonding," *Appl. Phys. Lett.*, vol. 68, no. 2609, pp. 2609–2611, 1996.
[8] A. Grisard, E. Lallier, and B. Gérard, "Quasi-phase-matched gallium arsenide for versatile mid-infrared frequency conversion," *Opt. Mater. Exp.*, vol. 2, no. 8, pp. 1020–1025, 2012.
[9] P. Liu, W. Shi, D. Xu, X. Zhang, G. Zhang, and J. Yao, "Efficient phase-matching for difference frequency generation with pump of Bessel laser beams," *Opt. Exp.*, vol. 24, no. 2, pp. 901–906, 2016.
[10] T. H. Stievater *et al.*, "Mid-infrared difference -frequency generation in suspended GaAs waveguides," *Opt. Lett.*, vol. 39, no. 4, pp. 945–948, 2014.
[11] C. R. Philips *et al.*, "Wide tunable midinfrared generation in orientation-patterned GaAs pumped with a femtosecond Tm-fiber system," *Opt. Lett.*, vol. 37, no. 14, pp. 2928–2930, 2012.
[12] D. F. Logan, M. Giguere, A. Villeneuve, and A. S. Helmy, "Widely tunable mid-infrared generation via frequency conversion in semiconductor waveguides," *Opt. Lett.*, vol. 38, no. 21, pp. 4457–4460, 2013.
[13] J. P. van der Ziel, M. Ilegems, and R. M. Mikulyak, "Optical birefringence of thin GaAs-AlAs multilayer films," *Appl. Phys. Lett.*, vol. 28, no. 12, pp. 735–737, 1976.
[14] A. Fiore, V. Berger, E. Rosencher, N. Laurent, N. Vodjdani, and J. Nagle, "Huge birefringence in selectively oxidized GaAs/AlAs optical waveguides," *Appl. Phys. Lett.*, vol. 68, no. 10, pp. 1320–1322, 1996.
[15] E. Guillotel *et al.*, "Parametric amplification in GaAs/AlOx waveguide," *Appl. Phys. Lett.*, vol. 94, no. 17, pp. 1110-1-1110-3, 2009.
[16] A. Fiore, V. Berger, E. Rosencher, P. Bravetti, and Nagle, "Phase matching using an isotropic nonlinear optical material," *Nature*, vol. 391, pp. 463–465, 1998.
[17] W. Cai and V. M. Shalaev, *Optical Metamaterials: Fundamentals and Applications*. Berlin, Germany: Springer, 2009.
[18] J. Elser, R. Wangberg, and V. A. Podolskiy, "Nanowire metamaterial with extreme optical anisotropy," *Appl. Phys. Lett.*, vol. 89, no. 26, pp. 1102-1 102-3, 2006.
[19] J. Yao *et al.*, "Optical negative refraction in bulk metamaterials of nanowires," *Science*, vol. 321, p. 930, 2008.
[20] Y. Liu, G. Bartal, and X. Zhang, "All-angle negative refraction and imaging in a bulk medium made of metallic nanowires in the visible region," *Opt. Exp.*, vol. 16, no. 20, pp. 15439–15448, 2008.
[21] A. Fang, T. Koschny, and C. M. Soukoulis, "Optical anisotropic metamaterials: Negative refraction and focusing," *Phys. Rev. B*, vol. 79, no. 24, pp. 1–7, 2009.
[22] J. B. Pendry, A. J. Holden, and W. J. Stewart, "Extremely low frequency plasmons in metallic mesostructures," *Phys. Rev. Lett.*, vol. 76, no. 25, pp. 4773–4776, 1996.
[23] B. Pendry *et al.*, "Low frequency plasmons in thin-wire structures," *J. Phys., Condens. Matter*, vol. 10, pp. 4785–4809, 1998.

[24] G. D'Aguanno, N. Mattiucci, A. Alù, C. Argyropoulos, J. V. Foreman, and M. J. Bloemer, "Thermal emissions from metamaterial wire medium slab," *Opt. Exp.*, vol. 20, no. 9, pp. 9784–9789, 2012.
[25] P. A. Belov *et al.*, "Strong spatial dispersion in wire media in the very large wavelength limit," *Phys. Rev. B*, vol. 67, no. 11, pp. 1–4, 2003.
[26] V. G. Dmitriev, G. G. Gurzadyan, and D. N. Nikogosyan, *Handbook of Nonlinear Optical Crystals*, 3rd Revised Edition. Berlin, Germany: Springer, 1999, pp. 17–30.
[27] S. Shingubara, "Fabrication of nanomaterials using porous alumina templates," *J. Nanoparticle Res.*, vol. 5, pp. 17–30, 2003.
[28] N. R. de Tacconi and K. Rajeshwar, "Semiconductor nanostructures in an alumina template matrix: Micro versus macro-scale photoelectrochemical behavior," *Electrochimica Acta*, vol. 47, pp. 2603–2613, 2002.
[29] G. D. Sulka, L. Zaraska, and W. J. Ste˛pniowski, "Anodic porous alumina as a template for nanofabrication," *Encyclopedia Nanoscience Nanotechnol.*, vol. 11, pp. 261–349, 2011.
[30] M. A. Noginov and V. A. Podolskiy, *Tutorials in Metamaterials*. Boca Raton, FL, USA: CRC Press, 2012.
[31] T. Skauli *et al.*, "Improved dispersion relations for GaAs and applications to nonlinear optics," *J. Appl. Phys.*, vol. 94, no. 10, pp. 6447–6455, 2003.
[32] L. V. Alekseyev and E. Narimanov, "Slow light and 3D imaging with non-magnetic negative index systems," *Opt. Exp.*, vol. 14, no. 23, pp. 11184–11193, 2006.
[33] S. Anantha Ramakrishna, "Physics of negative index materials," *Rep. Prog. Phys.*, vol. 68, pp. 449–521, 2005.
[34] R. L. Sutherland, *Handbook of Nonlinear Optics*, 2nd ed. New York, NY, USA: Marcel Dekker, 2003.
[35] Y. Ma, X. Li, H. Yu, L. Tong, Y. Gu, and Q. Gong, "Direct measurement of propagation losses in silver nanowires," *Opt. Lett.*, vol. 35, no. 8, pp. 1160–1162, 2010.